Kinetic Methods for Predicting Flow Physics of Small Thruster Expansions

Deborah A. Levin *

The Pennsylvania State University,

University Park, PA 16802

USA

January 24, 2011

Contents

*Professor, Department of Aerospace Engineering, email address dalevin@psu.edu

1. REPORT DATE	2. REPORT TYPE	3. DATES COVERED
JAN 2011	**N/A**	**-**

4. TITLE AND SUBTITLE	5a. CONTRACT NUMBER
Kinetic Methods for Predicting Flow Physics of Small Thruster Expansions	5b. GRANT NUMBER
	5c. PROGRAM ELEMENT NUMBER
6. AUTHOR(S)	5d. PROJECT NUMBER
	5e. TASK NUMBER
	5f. WORK UNIT NUMBER
7. PERFORMING ORGANIZATION NAME(S) AND ADDRESS(ES) **The Pennsylvania State University, University Park, PA 16802 USA**	8. PERFORMING ORGANIZATION REPORT NUMBER
9. SPONSORING/MONITORING AGENCY NAME(S) AND ADDRESS(ES)	10. SPONSOR/MONITOR'S ACRONYM(S)
	11. SPONSOR/MONITOR'S REPORT NUMBER(S)

12. DISTRIBUTION/AVAILABILITY STATEMENT
Approved for public release, distribution unlimited

13. SUPPLEMENTARY NOTES
See also ADA579248. Models and Computational Methods for Rarefied Flows (Modeles et methodes de calcul des coulements de gaz rarefies). RTO-EN-AVT-194

14. ABSTRACT

15. SUBJECT TERMS

16. SECURITY CLASSIFICATION OF:			17. LIMITATION OF ABSTRACT	18. NUMBER OF PAGES	19a. NAME OF RESPONSIBLE PERSON
a. REPORT **unclassified**	b. ABSTRACT **unclassified**	c. THIS PAGE **unclassified**	**SAR**	**28**	

1   Introduction

Modeling of small thruster expansions has seen a sustained development of computational methods and options over the last decade. The physics of such flows encompasses multiple length-scales from continuum to rarefied as the gas expands through the nozzle into the near-space vacuum. Moreover, with the advent of MEMS fabrication both cold and hot gas working fluids experience non-continuum effects because the surface-to-volume ratio is higher than in traditional axi-symmetric nozzles. As MEMS fabrication has improved to enable higher stagnation pressures particle methods are still relevant. However, they must be able to take advantage of the large collision rates in the early part of the expansions, rather, than be penalized by enormous computational costs of DSMC. Finally, increasing the stagnation temperature does improve thrust levels (although not efficiency), but, predicting the sustainability of the nozzle material means that particle-flow and thermal simulations must be coupled.

Because the residence time of the gas from the nozzle throat to the exit is sufficiently short the chemistry of multi-species flows through meso and MEMS -scaled nozzles is essentially frozen. However, given the rapidly falling gas temperature caused by the strong supersonic expansion condensation both inside and beyond the nozzle exit are likely in many neutral gas flows. Whether the condensation is *homogeneous* or *heterogeneous* is an important question. From an operational point of view, heterogeneous condensation rates are orders of magnitude faster than homogeneous condensation, however, scientifically such processes are more difficult to model due to the lack of detailed information regarding trace impurities which initiate the process. Condensation is an important source of spacecraft contamination and in such a context can only be studied using particle approaches.

The research that has been conducted in my group has sought to address the above technical challenges and issues and will be summarized in these lecture notes. It should be stated from the out set that the modeling of MEMS and small nozzle thruster simulations using particle and continuum approaches has been carried out by others, notably Ivanov,(1) Gimelshein and Wysong,(2) Aleexenko,(3) and others and the experimental endeavors to provide modelers with important thrust measurements include the work of Kestdever,(4; 5) Hitt,(6), for example. Due to the lack of time, these notable contributions will not be summarized although an attempt will be made to provide appropriate attribution. The author apologizes in advance for any omissions. The organization of the lecture is as follows. After discussing the numerous applications of modeling supersonic expansions for finite Knudsen number flows, the inter-relationships among the different types of particle computational tools used in the research here is discussed. Then the physics of two important types of expanding flows are examined. First we discuss MEMS flows for simple gases. We then discuss what we have learned from our modeling of condensing flows covering the spectrum of chemically inert or argon flows through small polyatomic systems such as water, carbon dioxide, ammonia, and ethanol. Conclusions in terms of anticipated future directions and challenges are then presented.

2 Particle methods Computational Tools

2.1 DSMC and Collision-limiter Techniques

The direct simulation Monte Carlo method first proposed by Bird(7) is frequently described as a phenomenological approach for simulation of rarefied gas flows by modeling the motion of fictitious particles. The correct usage of the DSMC method requires time and space discretization in sufficiently small quantities to ensure that the predicted flow parameters correspond to a solution of the Boltzmann equation. The latter is the most general equation to describe the transport of gases in a fully kinetic manner. DSMC is a numerical approach for solving the Boltzmann equation, an integro-differential equation that in general is not amenable to analytic solution, if the gas is dilute, composed of binary collisions and molecular chaos holds. As has been discussed by Ivanov and Rogasinky(8) and later Alexeenko,(9) the phenomenological description of the method is not necessary. The two widely used approximate numerical schemes for the collisional relaxation used in the direct simulation Monte Carlo method are the No Time Counter (NTC) due to Bird(7) and the Majorant Frequency Scheme (MFS) of Ivanov and Rogasinky. Both schemes have the same numerical efficiency, with computational cost linearly proportional to the number of particles, N instead of N^2. The MFS, however, is more accurate than NTC because it allows one to model the collisional relaxation with a smaller number of particles.

The MFS relaxation scheme during a time step, Δt can be summarized as follows. The initial state $\vec{C}_0$ is selected from the probability density $f_N(\vec{C}, 0)$ where the velocities of N particles can be described by,

$$\vec{C} = (\vec{v}_1, \vec{v}_2, ...\vec{v}_N)$$

and $f_N(\vec{C}_1, t)$ is the the probability density for the stochastic vector $\vec{C}$ to have value the value $\vec{C}_1$ at time t. Then the time between two collisions, τ_m, is determined by setting

$$\tau_m = -\nu_m^{-1} \ln rand \tag{1}$$

where ν_m is the majorant frequency. The time counter within the time step is increased by

$$t_{n+1} = t_n + \tau_m$$

and if $t_{n+1} > \Delta t$ then no more particles are selected for collisions in the present time step. Else, a new pair of particles with velocities (v_i, v_j) are selected from the system of N particles if,

$$rand < \frac{g_{ij}\sigma(g_{ij})}{[g_{ij}\sigma(g_{ij})]_{max}}$$

where g_{ij} is the relative collision velocity and σ is the collision cross section. If the inequality holds then the selected pair is allowed to collide and they obtain new velocities after the collision of $(v_i\prime, v_j\prime)$. Else one determines the time of the next collision.

It should be noted that unlike the Navier-Stokes equations, the Boltzmann equation of transport is valid over *all* flow regimes. In the high-collision limit, or the very low Knudsen number limit, the Boltzmann equation can be shown using Chapman-Enskog

theory to reduce to the Navier-Stokes and Euler's equations. Since the Knudsen number may be related to the Mach and the Reynolds numbers the selection of whether the Navier-Stokes or the Euler's inviscid flow equation is appropriate depends on the degree of viscosity in the flow. In particular, if the flow is inviscid the Knudsen number approaches zero, all collisions are perfectly elastic and reversible, and the distribution function is the equilibrium Maxwell-Boltzmann velocity distribution function. While this is an idealization, the core region in a supersonic nozzle expansion is a good example of where such a situation physically occurs. A great deal of computation time can be saved if one knows a priori that equilibrium occurs after some specified number of collisions (*i.e.,* the collision limiter or enforcer) and the MFS algorithm can be naturally adapted to implement this procedure within a time step within a DSMC cell as follows. Using the same initial state as above, select particles subject to the inequality given by Eq. 1. If the selected pair satisfies the inequality perform a collision and assign new velocities as in the MFS procedure. If not, select another pair and use Eq. 1 to test again until the necessary number of collisions (as specified by the collision limiter number) have been performed. When so accomplished, move on to the next cell and time step. This procedure is the simplest of "reduced DSMC" particle methods and is known as the "eDSMC" method where the 'e' stands for equilibrium.(10) This approach was developed to try to extend the range of stagnation pressures for which DSMC could be used to model MEMS and small meso-thruster size flows. The approach was successful in evaluating the nozzle thrust for a variety of MEMS shapes and stagnation conditions (11), however, it proved insufficiently accurate for modeling regions of the flow in the vicinity of the nozzle wall where sizeable viscosity exists.(12) For this reason we proceeded to examine the more accurate particle techniques discussed below.

2.2   BGK Approaches

Although we tend to develop computational techniques by artificially choosing problems where we know they will work, reality forces us back to the situation where ultimately no single approach will be feasible. In particular, micro- and meso- nozzle transitional flows exhibit strong thermo-chemical non-equilibrium with regions that are very continuum and others that are very rarefied. Different investigators have recognized this problem as well and have proposed uncoupled NS/DSMC approaches where the NS equations were used to model the high density portions in the nozzle and the DSMC was used to predict the rarefied plume-atmospheric interaction.(13) This approach while demonstrated to be useful, has the draw back that a starting surface must be created in the supersonic region and the geometry should be well defined in order to keep the generation of the starting surface tractable. For condensing flows, it requires one to make the further assumption that the supersaturation ratio remains below unity upstream of the starting surface. This condition is not certainly not guaranteed for all stagnation pressure and nozzle conditions. Since our goal is to "hybridize" DSMC and BGK approaches we have emphasized the particle-based formalism of the BGK approach rather than finite volume formulations.(14)

The BGK method is a technique that approximates the solution of the Boltzmann

---

equation,

$$\frac{\partial}{\partial t}(nf) + v \cdot \frac{\partial}{\partial \vec{r}}(nf) + \vec{F} \cdot \frac{\partial}{\partial \vec{v}}(nf) = \int_{-\infty}^{\infty} \int_{0}^{4\pi} n^2 \left(f^* f_1^* - f f_1\right) v_r \sigma d\Omega d\vec{v} \qquad (2)$$

where f and f_1 are the pre-collision single particle velocity distribution functions of the two colliding particles and f^* and f_1^* are their post-collision velocity distribution functions; $\vec{F}$ is an external force per unit mass applied to the particles (assumed to be zero for the present study); σ is the differential cross-section of the binary collision and Ω is the solid angle; v_r is the relative velocity of the colliding particles, and n is the number density.

To understand the BGK model, let us concentrate on the collision term on the right hand side of Eq. 2 that is difficult to compute because it involves multiple integrations. Different simplified models have been proposed to model this complicated collision term with one such simplified model expressing the collision term in a relaxation form known as the Bhatnagar-Gross-Krook (BGK) model:

$$\left[\frac{\partial}{\partial t}(nf)\right]_{collision} = \nu n(f_e - f) \qquad (3)$$

where n is the number density, ν is the characteristic relaxation frequency and f_e is the Maxwellian distribution function. Thus the BGK model is a simplified linear approximation to the nonlinear collision term of the Boltzmann equation and provides an alternate procedure to account for the collisional process driving a flow toward equilibrium without modeling individual collisions. This simplification is reasonable for flows with large collision rates since the details of the particle interactions are not significant in reproducing macroscopic quantities such as temperature, pressure or flow velocity(15). Because the BGK equation reproduces correct moments and satisfies the H-theorem for entropy production, it is accepted as an accurate physical model of high density flows that we will discuss here.

To compute the collision term in the BGK model, we first need to define the rate at which the flow relaxes toward equilibrium. For each species, the relaxation rate is governed by the respective characteristic relaxation frequency given by

$$\nu = \text{Pr} \cdot nk \left(\frac{T_{ref}^{\omega}}{\mu_{ref}}\right) T_t^{1-\omega} \qquad (4)$$

where Pr is the Prandtl number of each species (assumed to be unity for the BGK equation), k is the Boltzmann constant, T_t is the local translational temperature in a cell, and μ_{ref} is the gas dynamic viscosity of each species at T_{ref}.

In each cell, the number of particles selected for each species for the velocity sampling from the local Maxwellian distribution depends on the relaxation frequency of the corresponding species and the time step, and given by

$$N_c = \text{int}(N(1 - \exp(-\nu\Delta t)) \qquad (5)$$

where Δt is the time step, N is the number of particles of each species in a cell and the *int* operator means the nearest smaller integer.

The particles, which have been selected for velocity sampling, are assigned new thermal velocities according to the Maxwellian distribution at the local cell based temperature.

$$v_x^1 = \cos(2\pi R_1)\sqrt{-\ln(R_2)} \cdot \sqrt{2kT_t/m} \tag{6}$$

$$v_y^1 = \sin(2\pi R_1)\sqrt{-\ln(R_2)} \cdot \sqrt{2kT_t/m} \tag{7}$$

$$v_z^1 = \cos(2\pi R_3)\sqrt{-\ln(R_4)} \cdot \sqrt{2kT_t/m} \tag{8}$$

where R_1 through R_4 are random numbers uniformly distributed between 0 and 1 and the superscript 1 indicates the velocity after the assignment of new thermal velocities. The velocities of particles which have not been preselected remain unchanged in the current time step.

Holway(16) and Cercignani(17) proposed a modification to the BGK equation, so as to produce the correct transport coefficients of heat transfer and viscosity. The equilibrium distribution function in the ES-BGK model is the local anisotropic three-dimensional Gaussian, f_G, referred to as the Ellipsoidal Statistical (ES) distribution, and the collision term is approximated as

$$\left[\frac{\partial}{\partial t}(nf)\right]_{collision} = \nu n(f_G - f) \tag{9}$$

The sampled velocities from the BGK procedure are modified to new values conforming to the ES distribution as follows:

$$v_i^2 = S_{ij} \cdot v_j^1 \tag{10}$$

where $\overrightarrow{v^2}$ designates the modified velocity components and S_{ij} is given by the following equation:

$$S_{ij} = \delta_{ij} - \frac{1-Pr}{2Pr}\left[\frac{1}{kT_t}\frac{N}{N-1}\left(<mv_iv_j>_a - <mv_i>_a<mv_j>_a \,/\, <m>_a\right) - \delta_{ij}\right] \tag{11}$$

where the symbol $<>_a$ represents an averaging over all the particles in a cell, δ_{ij} is the Kronecker delta, m is the mass of a particle, and indices i, j refer to the three Cartesian components of velocity.

Similarly, particles of each species involved in the flow field are selected for the rotational and vibrational energy relaxation. The corresponding relaxation frequency is given by the following equation

$$\nu_r = \frac{F_{coll}}{Z_r}, \quad \nu_v = \frac{F_{coll}}{Z_v} \tag{12}$$

where F_{coll} is the collision frequency for every species involved, and given by the following equation

$$F_{coll} = \frac{4}{n}\sqrt{\frac{kT_{ref}}{2\pi}}\left[\frac{T_t}{T_{ref}}\right]^{1-\omega}\sum_{i=1}^{N_{spec}}\sum_{j=1}^{i}n_in_jA_{ij}\left(2-\delta_{ij}\right) \tag{13}$$

where n is the overall number density, $n = \sum_{i=1}^{N_{spec}} n_i$

$$A_{ij} = \frac{\pi}{4}\left(d_{ref,i} + d_{ref,j}\right)^2\sqrt{\frac{m_i+m_j}{m_im_j}} \tag{14}$$

In Eq. 12, Z_r is computed individually for every species using the modified Parker (18; 19) formula.

$$Z_r = \frac{3/5 Z_r^\infty}{1 + (\pi^{1/2}/2 \, (T_t^*/T_{eq})^{1/2} + (\pi + \pi^2/4) \, (T_t^*/T_{eq})}$$

(15)

where T_{eq} is the equilibrium temperature given by

$$T_{eq} = \frac{F_t T_t + F_r T_r + F_v T_v}{F_t + F_r + F_v}$$

(16)

where F_t, F_r and F_v are the degrees of freedom for translational, rotational and vibrational modes, and T_t, T_r and T_v are translational, rotational and vibrational temperatures respectively.

The constants T^* and $Z_r{}^\infty$ involved in Eq. 15 are referred to as characteristic temperature and maximum rotational collision number of a polyatomic species. For CO_2, the values of T^* and $Z_r{}^\infty$ used in the present work are 91.5 K and 18.5 respectively. The vibrational collision number for CO_2 is assumed to be related to the rotational collision number by the following relation, $Z_v = Z_r/5$.

Once we have computed relaxation frequency for rotational and vibrational equilibrium, we can find out the number of particles for each species to be selected for rotational and vibrational relaxation from the following equations respectively, which are in nature similar to the Eq. 5.

$$N_r = \text{int}(N(1 - \exp(-\nu_r \Delta t))$$

(17)

$$N_v = \text{int}(N(1 - \exp(-\nu_v \Delta t))$$

(18)

In the present work, for rotational and vibrational relaxation, the particles are selected from those selected for velocity sampling, i.e., among N_v particles of each species.

A comparative study of the DSMC and statistical BGK and ES-BGK methods was carried out in Ref. (12) by simulating a supersonic expansion of argon to vacuum in a nozzle for different pressure cases and comparing with the DSMC solution as the benchmark. Statistical BGK and ES-BGK methods were found to be in good agreement with the benchmark DSMC method with ES-BGK method showing a better agreement. It was also shown that the statistical methods of solving the BGK equation were four times more numerically efficient than the deterministic finite volume BGK method and twice as efficient as the DSMC method. Another comparative study was carried out in Ref. (20) to estimate the accuracy of the statistical BGK and ES-BGK methods for a multi-species case involving involving the modeling of reinforced carbon-carbon (RCC) thermal protection system crack growth using kinetic BGK method for internal and external flows. Statistical BGK method was found to be in good agreement with the DSMC method for the external flows. For modeling the internal flows (with high local pressure) within the vicinity of crack, only the BGK method was applied, because of its cost effectiveness for the high pressure flows. Finally, as will be discussed in later sections, our implementation of the BGK method has allowed us to extend our DSMC-based condensation modeling to higher nozzle pressure conditions.

2.3   Molecular Dynamics

In contrast to the aforementioned computational techniques molecular dynamics (MD) is not a statistical method. Every particle is assumed to represent a *single* true physical particle and the outcome of every collision is based on the potential energy curve in contrast to DSMC which assumes that the outcome is statistical, although based on a realistic cross section. The collision dynamics are purely deterministic and obtained by the integration of Hamilton's questions.(21) MD is not limited therefore to the binary and dilute gas assumption so that it can be applied to a system of particles in either the solid, liquid, or gaseous phase. Because the entire trajectory is modeled the typical applicability of MD is for a system of size on the order of a nm with 10^6 particles, and for a time scale of ~ 100 ps, , *i.e.,* systems much smaller in scope that are considered by DSMC or its related particle approximations. In our work we have used MD as a method of modeling the "fine-grained" physics of the problem, *i.e.,* to obtain state-specific reaction cross sections, improvements to the VHS total cross section, and develop gas-cluster phase collision and interaction models that may be used in "course"-grained DSMC and related particle approaches.

3   Modeling of MEMS Thrusters

With almost nine orders of magnitude difference between conventional and MEMS nozzle thrusters there is no reason to expect that the physics of the latter should be the same as the former. In fact, it is not. For the MEMS devices that will be discussed in this paper, the nozzle geometries are both rectangular and axi-symmetric. Figure 1(a) shows a comparison of the stream wise velocity, $u/u(0)$, normalized by the value along the nozzle axis, across the exit of a 3-D MEMS nozzle at the nozzle exit with a conventional nozzle. The combination of the geometry and the highly viscous flow creates a boundary layer which can be seen to substantially envelop the core flow. The surface affects due to wall temperature, heat transfer, and heat flux are substantial and will be shown to be controlling factors for micronozzle performance and system design. The right hand portion of the figure shows the development of the boundary layer in a three-dimensional micronozzle for a cold gas flow at different axial locations from the nozzle throat. It can be seen that at the exit the thermal boundary layer engulfs the entire flow for these conditions. Yet fabrication of such systems in silicon and other materials is well advanced and concepts such as those proposed by Reed and co-authors(22) shown in Fig. 2 have been achieved. The figure shows an array of thrusters fabricated on a silicon chip with different thruster sizes (throat areas, nozzle area ratios) available for a range of thrust levels (from μ-N to mN) within the same array. Several thrusters can be fired simultaneously for thrust levels higher than the basic units, or in a rapid sequence in order to provide gradual but steady low-g acceleration. Decomposing solid propellant pellets would be loaded into each thruster prior to bonding the half sections. Decomposing solids, also referred to as gas generators, are slow-burning propellants designed for maximum gas yield. Initiation of the propellants would be accomplished with a diode laser-based, fiber-optic network. A critical portion of our research activity was the use of DSMC to model the nozzle design because it was recognized that it will be critical to the performance of the system.
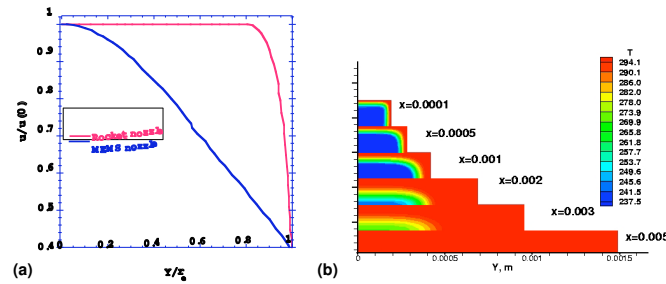
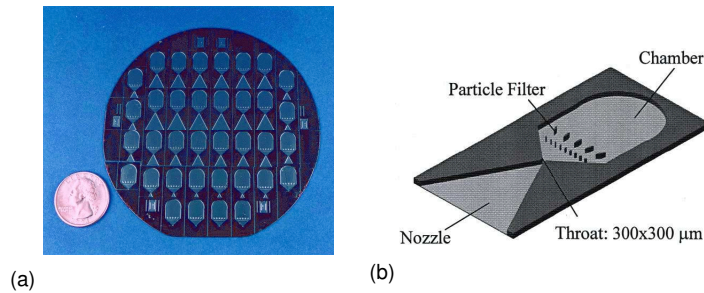Figure 1: Comparison of traditional and MEMS nozzle boundary layer growth.

Figure 2: MEMS fabrication concept of an array (a) and a single (b) thruster.(22)

The DSMC simulations were performed to understand in detail the interaction of nozzle-shape, wall temperature, and stagnation pressure and temperature effects on nozzle efficiency, specific impulse, and thrust. We start with the modeling of cold gas thrusters considering the affect of three vs. the approximate two-dimensional model. Then we consider whether better nozzle performance is obtained for higher temperature stagnation conditions. Finally, we examine high-temperature gas thrusters with variable wall temperatures by use of coupled DSMC/finite-element method (FEM) heat transfer simulations considering both the affect of heat transfer on the thruster performance as well as the material structural survivability.

Results from various DSMC simulations will be presented below. Depending on the stagnation pressure, typical DSMC simulations require about 2.8 to 15 million particles, with time steps on the order of 1 nsec to reach convergence. Due to the large computational cost to perform a simulation of the true three-dimensional structure, approximate two-dimensional and axisymmetric structures were considered and compared with the 3-D results to understand the implications of using these approximate geometries.

3.1   Cold Gas Thrusters

Figure 3 shows the three nozzle geometries that were considered in our studies. The left hand portion of the figure shows a three-dimensional nozzle of a 15-deg expansion angle in the XY plane, a throat width and height of 300 μm, and an area ratio of 10. A two-dimensional approximation can be constructed from this geometry by neglecting the end surfaces of the nozzle and assuming that the height or separation of the side walls is very

large. Similarly, an axisymmetric geometry (RHS of Fig. 3) was also considered keeping the expansion angle the same as in the two and three-dimensional nozzle geometries but using a throat radius of 150 μm with an exit to throat area ratio of 100. The test gas was molecular nitrogen with stagnation temperature and pressures of 300 K and 10 kPA, a wall temperature of 300 K, a Kn=.005 and a Re of 200. Figure 4 shows a summary of some of the important results from our previous studies.(23) The comparison of the 3-D versus the approximate 2-D geometry for gas density and temperature shows that the 2-D geometry is not a good approximation for the real 3-D configuration. The 2-D flow exhibits a higher expansion and thinner thermal boundary layer due to less heat transfer to the nozzle walls compared to the 3-D geometry. A similar conclusion is reached when comparing the 3-D versus the axisymmetric temperature and velocity profiles. The surface area to volume ratio is less for the axisymmetric case than the 3-D geometry, and, again the temperature drop and velocity increase of the axisymmetric case are more consistent with isentropic supersonic expansions. In contrast, the 3-D geometry does not have a maximum velocity at the exit and instead of the temperature monotonically falling it actually increases as the flow approaches the exit. Further examination of thruster performance(23) showed that the additional wall effects in the 3-D geometry reduce thrust by about 20% compared to the 2-D case.
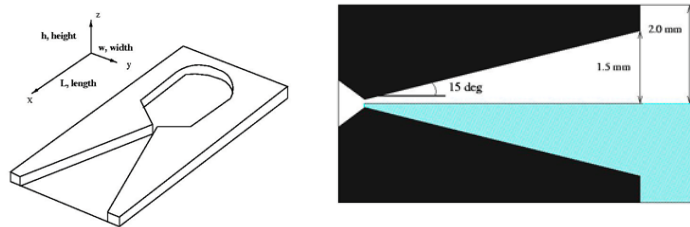

Figure 3: Cold gas thruster geometries (a) 3-D flat nozzle (b) Axisymmetric nozzle.(22)

3.2   Heated and High Temperature Gas Thrusters

In this portion of the research we examined the sensitivity of MEMS thruster flows, with the same or similar geometry from the previous subsection, to increases in the stagnation temperature. As we increase the stagnation temperature we expect that the thrust would increase for the same wall nozzle. However, the increase in thrust is not similar to that which is observed in traditional propulsion systems. Starting with the velocity profiles for two different stagnation conditions of 300 versus 1,000 K, Fig. 5(a) shows that the velocity profiles change, but, for both temperatures the profiles are dominated by surface interactions for a 3-D nozzle with full wall accommodation, a throat Reynolds number of about 200 and a wall temperature of 300 K. The specific impulse for these two cases is 57 and 61 s for stagnation temperatures, T_o, of 300 and 1,000 K, respectively. Although there is an increase in specific impulse it is much less than would be observed for the comparable axisymmetric cases because the 3-D nozzle has a larger surface-area to volume ratio. Any factors which lead to an increase in the thermal boundary layer, mitigate the utility of the nozzle to further accelerate the flow and therefore produce thrust.
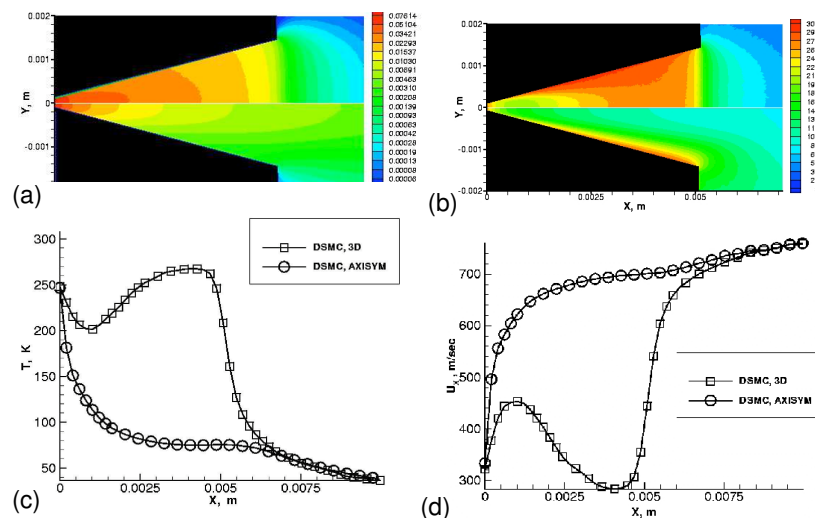
Figure 4: Cold gas thruster results. Portions (a) and (b) show a comparison of the flows for a 3-D (top) and a 2-D (bottom) geometry for gas density (kg/m^3) and temperature (K), respectively. Portions (c) and (d) show a comparison of the temperature profiles and stream wise velocity, respectively, along the nozzle axis from the throat to a region downstream of the exit for the 3-D versus an axisymmetric geometry.

This can be seen very clearly in Fig. 5(b). To reduce the computational effort (at that time) the ratio of the thrust to the thrust at the nozzle throat is shown as a function of distance, normalized by the throat radius, for an axisymmetric nozzle at three different stagnation temperatures, assuming a diffuse, isothermal wall at 300 K. The figure shows that as the stagnation temperature is increased the nozzle loses its ability to accelerate the flow and one should probably consider a shorter nozzle at higher stagnation temperatures for operation in the flow regime of Reynolds numbers of about 200 to 400. A similar trend(23) was observed in other calculations that we performed for the same axisymmetric nozzle but varying the stagnation pressure for a stagnation temperature of 2300 K. We found that the lower pressure (*i.e.*, more viscous flow) has a peak I_{sp} closer to the nozzle throat, again suggesting that a shorter nozzle would be more useful.

3.3   Coupled Gas-Material Simulations

As the above results and others presented in Ref. (23) show, the nozzle wall temperature and heat fluxes are major factors that influence the gas dynamics and micro-thruster performance. The actual burn time of a thruster is certainly an important design parameter that determines the impulse bit that will be available for a propulsion maneuver. In addition, heating the microstructure structure beyond its melting point will certainly limit its operation. For this reason we developed an approach to simulate the coupled thermal and gas dynamics. Since the Biot number is sufficiently small for a microscale device the lumped-capacitance method was used to estimate a material response time constant on the order of 0.01 s. This value is five orders of magnitude slower than the typical resi-
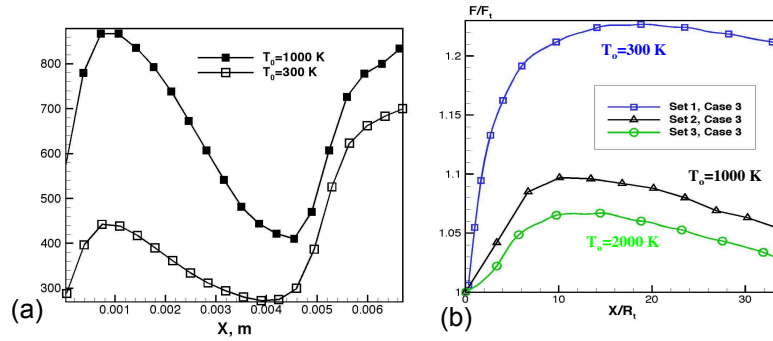
Figure 5: Warm gas thruster results. Portion (a) shows the streamwise velocity distribution along the nozzle axis for two stagnation temperature conditions for a three-dimensional nozzle and (b) shows a comparison of the thrust ratio for axisymmetric nozzles at three different temperatures.

dence time of the gas in the micro-nozzle, *i.e.,* 10^{-7} s, so that the two calculations may be loosely coupled.(24; 25) The coupling between the material thermal response and the DSMC flow occurs when the DSMC heat fluxes are used as boundary conditions for the heat conduction problem. The heat conduction calculation then gives a new wall temperature which is used in the next DSMC simulation. Figure 6(a) shows the finite element domain and its overlap with the micronozzle gas dynamic domain. The 3-D mesh for the 3-D nozzle used about 1600 nodes and about 7300 tetrahedral elements.

Figure 6(b) and (c) shows the gas and material temperature variation as a function of burn time for a 3-D nozzle with a stagnation pressure of 0.1 atm and an initial wall temperature of 300 K for two different thermal boundary conditions. The thermally insulated case corresponds to zero convective and conductive heat fluxes. The material (silicon) and the thruster boundary layer are isolated. The second condition of active cooling simulates the presence of laminar water cooling in microchannels (26) around the perimeter of the rectangular material shape. Comparison of the two sequences of simulations shows that in both cases the nozzle material temperature increases with time, but, cooling the outer surface of the thruster allows the material to remain at a temperature that is lower than the melting temperature. Therefore such a micro-thruster would achieve a longer thruster burn time. The gas flowfields change as well with time. In the insulated case the thermal boundary layer growth is higher than in the cooling case, although, it is difficult from the figures to discern this trend quantitatively.

Instead, the difference in the growth of the thermal boundary layer for the two thermal boundary conditions can be better seen in terms of the change in thrust and coefficient of mass discharge shown in Fig. 7. It can be seen that for either thermal boundary condition the thrust level falls as the material temperature rises, however, in the cooling case the material reaches a steady state condition with the drop in thrust only about 6% compared to the larger drop in thrust of $\sim$ 15% for the insulated case. Also shown is the change in the mass discharge coefficient as a function of time. Unlike the thrust, this coefficient is mainly affected by the growth of the boundary layer. The more the boundary layer
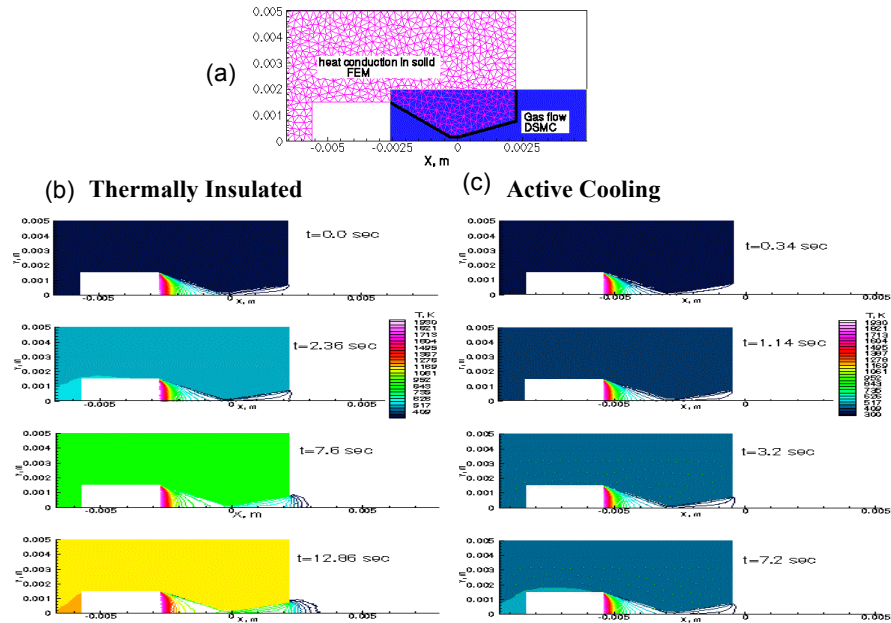
Figure 6: Coupled thermal and gas dynamic computations. (a) cross section of computational domains and time variation of temperature and material responses for the 3-D nozzle and a stagnation pressure of 0.1 atm for a thermally insulated boundary condition (b) and active cooling (c).

grows, the smaller is the effective cross sectional area of the nozzle and hence the discharge coefficient decreases. For an insulated nozzle the drop is as much as 55% of the initial value compared with only about 8% for the cooling case. The amount of flow energy that is lost to the wall in the form of heat can be estimated by examining the total heat fluxes (sum of kinetic and internal energy) through a cross section perpendicular to the nozzle axis. For the cooling boundary condition, a non-adiabatic case, the energy flux is not conserved and decreases along the nozzle axis. Figure 4.20 of Ref. (9) shows that as the material heats up less energy can be transferred to the wall which in turn reduces the decrease in thrust at later burn times. The main reason that the thrust decreases in time is due to the decrease in the mass discharge coefficient. These results show that the large temporal variation in thrust and mass discharge coefficient means that the coupling of the gas flow and material response has to be taken into account in serious micro-propulsion design efforts.

4   Condensation in Meso-scale Expansions

In this section we turn to the second important physical aspect in small thruster expansions, namely condensation. Our focus now turns away from the physics of the viscous boundary layer and is instead more on understanding the extreme supersonic expansion
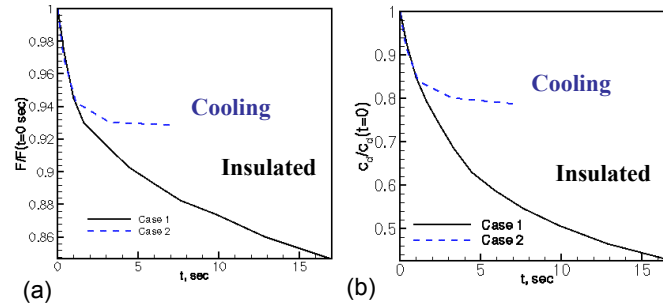
Figure 7: Influence of material response on micronozzle performance for a 3-D nozzle. Normalized thrust and coefficient of mass discharge a function of time.

and its affect on condensation. The effect of the boundary layer is of course still there and plays a critical role in modeling the nozzle lip region. Only a kinetic method can correctly model the mass flux in the back flow which entrains condensates that can coalescence and stick to a cold spacecraft surface.

There are a number of important challenges in modeling homogeneous condensation. The first and foremost are the multiple length scales in the problem due to expansion of the high pressure gas from the plenum to the space near-vacuum. Figure 8(a) shows the three order of magnitude variation in the Knudsen number from the nozzle throat to beyond the exit as a function of distance from the throat. As the flow expands the pressure drops and the supersaturation ratio, the ratio of the saturation pressure to the gas pressure, increases by orders of magnitude, with the axial variation depending on the specific chemical species, as shown in Fig. 8(b). DSMC cannot model the entire flow and the notional sub-divisions where other approaches might be used are shown below as the flow expands for an argon flow through an orifice. To cover the wide range of physical phenomena one needs both coarse grained and fine-grained computational techniques. DSMC is a logical choice for the coarse grained approach, but, the question still remains about how we can handle the high pressure region. As will be shown we have successfully used the BGK approach to model the plume from the nozzle exit to the farfield. Most likely future hybrid/DSMC methods will open up more opportunities to model non-laboratory condensating flows. However, regardless of the choice of coarse-grained gas dynamic approach, the appropriate physical condensation models are required. (Note that their specific implementation *will be* different, however.) We have sought to use fine-grained approaches such as molecular dynamics to provide mechanisms and models for cluster processes off-line as input for DSMC and BGK approaches. However, the MD results will only be as good as the inter-molecular potential so that the question arises as to whether there are adequate potential energy surfaces for even small, highly polar polyatomic systems. Finally, abundant data exists to validate condensating flows from small orifices and nozzles, but, much of it emphasizes terminal cluster sizes and number densities only.(27; 28)

In this section we briefly outline the important processes in condensating flows and the two approaches that we have used for developing condensation models, classical nucleation
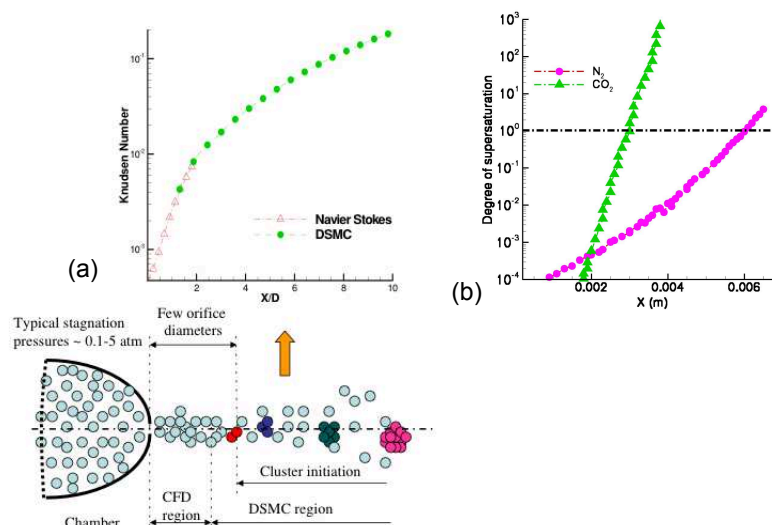
Figure 8: Challenges of modeling multi-scale condensing flows. (a) Knudsen number varies by at least three orders of magnitude causing the saturation ratio (b) to increase rapidly to greater than unity.

theory (CNT) and MD. Then we provide selected examples of how we have used these models in both DSMC and BGK simulations. In particular we will discuss our modeling results of carbon dioxide condensation and comparisons with the experiments of Ramos *et al*(29). This comparison with this data is important because it provides a test of both the nozzle near and far-field cluster size and density distributions obtained from the simulations. We then consider a *heterogeneous* condensation case where gases of molecular nitrogen and carbon dioxide with different saturation ratios are both present in an expanding jet plume. Molecular dynamics was used to calculate the sticking rate and the simulations are compared with Rayleigh scattering results. Finally, we end with an example of simulating ethanol data where we show that the use of the BGK approach is critical in enabling direct comparison with the data of Wegener *et al*.(30) Other systems that we have examined extensively include water(31; 32) and ammonia.(33) The ammonia system was interesting because the condensation occurs inside the nozzle and molecular dynamics was used to check the fidelity of an empirical coalescence model. The cluster size distributions obtained from the DSMC simulations were found to be in good agreement with the data of Bobbert *et al*.(34)

4.1   Condensation Processes

First and foremost it should be mentioned that condensation changes the plume flowfield distribution. Figure 9 shows the DSMC predicted plume temperature and mass fraction of water gas for the Progress main engine rocket plume with and without the modeling of water condensation at 300 km.(35) The Progress Main Engine conditions were modeled assuming a stagnation pressure of approximately 350 kPa, a stagnation temperature of 3800 K and a water species mole fraction at the nozzle exit of 28.95.% Figure 9(a) shows

that the condensation process increases the plume gas temperature The latent heat generated during the condensation process is released into the plume gases and increases its temperature. Figure 9(b) shows that downstream of the onset of condensation, about 3.6 m on the centerline, the total gas mass density in the condensation plume is less than that in the plume modeled without condensation. The reason for the decreased total gas mass density is that a large fraction of water molecules condense into clusters.
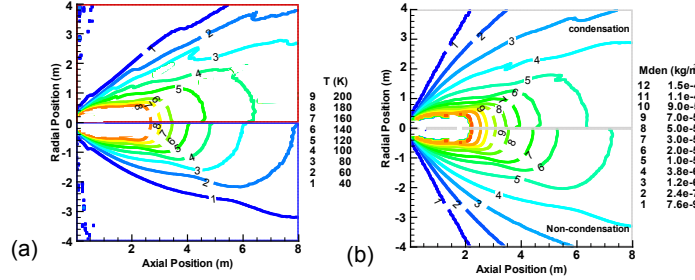

Figure 9: Comparison of temperature (a) and plume gas mass density (b) fields for a Soyuz rocket plume simulated with condensation (top) and without water condensation (bottom).

The processes that occur in a condensing flow include nucleation or creation of clusters, evaporation, sticking (cluster-monomer collisions), and coalescence (cluster-cluster) collisions. In the modeling of condensation processes in expanding supersonic jets the fidelity of the nucleation process is key. The easiest and most pervasive formalism to describe cluster nucleation is known as classical nucleation theory (CNT).(36; 37) The main idea behind CNT is that clusters smaller than a critical size (based on thermodynamic parameters) will be unstable and that clusters larger than the critical size will spontaneously grow in a supersaturated environment. The critical size, $r*$, is given in CNT as,

$$r* = \frac{2\sigma}{\rho RT \ln S}, \quad S = \frac{p}{P_s} \tag{19}$$

where σ is the surface tension, R is the universal gas constant, T is the gas temperature, P_s is the saturation pressure, and S is the saturation ratio. Other important relationships from CNT for the condensation (or sticking), the evaporation, and the nucleation rate are given respectively as,

$$C = \frac{4\pi r^2 qp}{\sqrt{2\pi mkT_g}}, \quad E = \frac{4\pi r^2 P_s}{\sqrt{2\pi mkT_c}} \exp\left(-\frac{\sigma}{\rho RT_c r}\right), \quad J = \sqrt{\frac{2\sigma}{\pi m^3}} \frac{\rho_g^2}{\rho_l} \exp\left(-\frac{4\pi r *^2 \sigma}{3kT}\right) \tag{20}$$

where ρ_l is the density of the liquid state, ρ_s is the density of the monomer or gaseous state, T_g and T_c are the temperatures of the gas and cluster, and q is the sticking probability. As the above relationships show, if one knows the thermodynamic properties such as surface tension, saturation pressure, and phase temperatures, the above rates are all defined. The problem is that implicit in the assumptions of the above rates is that the volume of gas has had a sufficient number of collisions to equilibrate (a long residence time), a condition that

is certainly not expected in many supersonic expansions to vacuum. Furthermore, if the conditions are such that the critical cluster size is small, it is not clear that the macroscopic surface tension can actually describe a small cluster such as a dimer, trimer, etc. In fact the CNT rate that was used in the aforementioned water condensation simulation of the Soyuz plume used the correction to the CNT nucleation rate of Wolk *et al.* Although the correction is motivated by experimental nozzle measurements it is problematic because for the conditions of the Soyuz plume simulation it varies by orders of magnitude and not in a consistent manner.

Even considering a gas simpler than water such as argon does improve the uncertainty involved in using the CNT nucleation rate. A *full kinetic nucleation* model for argon was implemented and incorporated into the DSMC.(38; 39) Figure 10 shows a comparison of the average cluster size (a) and the average cluster number density (b) predicted for the kinetic and CNT models for argon condensation. The change in the physics between the two nucleation models is evident from the strong different in the spatial dependence. The average cluster size is normalized to 50 and 1,000 for the kinetic and CNT models, respectively. The average cluster number density is normalized to 8×10^{20} and 8×10^{17} m^{-3}, for the kinetic and CNT models, respectively. The cluster number density contours for the simulation using the kinetic nucleation process is smoother than for the simulation using CNT because computation temperature *during* a DSMC calculation is an inherently noisy process. In addition, the cluster number density predicted by the kinetic nucleation model is about three to four orders larger than for CNT.
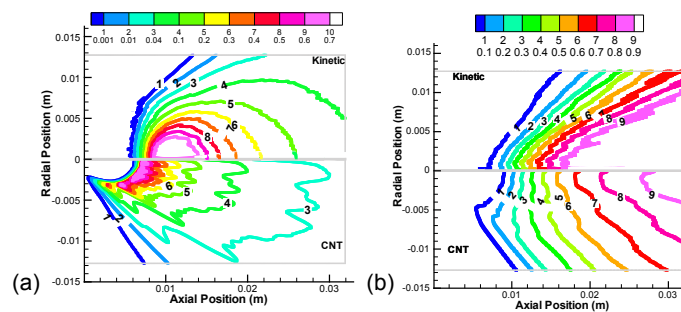

Figure 10: Portions (a) and (b) show the argon average cluster number density and average cluster size for two different nucleation models, respectively.

This comparison shows that whenever possible it is important to verify the fidelity of CNT and when good potential energy surfaces exists, MD is a good option. Such studies were carried out by Li *et al* to study water condensation in small jets using MD to obtain the nucleation mechanisms and rates and the sticking parameters as well.(31; 32) As stagnation pressure conditions increase, however, CNT becomes more of a viable option.

4.2   Carbon Dioxide Condensation

We present here our modeling of carbon dioxide condensation for the experimental conditions of of Ramos *et al*(29). In Ref. (40) the details of the pipe-shaped nozzle CFD modeling and the specific starting surface for the particle simulations are presented. A

comprehensive DSMC based condensation model taking into account the processes of nucleation, cluster-monomer sticking and non-sticking collision, and cluster evaporation was developed and compared with the experimental data(29) in terms of cluster size and number density distributions. The experimental data was obtained by Ramos *et al*(29) as part of their quantitative study of cluster growth in free-jet expansions of CO_2 for stagnation temperature of 294 K and stagnation pressures ranging from 1 to 5 bars. They used Rayleigh scattering and linear Raman spectroscopy techniques to obtain high spatial resolution of quantitative growth of clusters in supersonic jets of CO_2. The basic quantities measured along the jet were the intensities of Rayleigh scattering and of rotational and vibrational Raman lines from which cluster number density and cluster size distributions were derived. The work carried out in Ref. (40) involved simulation of condensation for stagnation pressures varying from 1 to 3 bars. and the comparison with the measured cluster number density and average size is shown in Fig. 11(a) and (b). It can be seen that the agreement between DSMC and experiment is reasonable for a stagnation pressure of 1 bar but is unsatisfactory for the higher stagnation pressures of 2 and 3 bar. DSMC numerical parameter requirements for higher stagnation pressures, such as 4 and 5 bar, could not be satisfied. Further comparison of the DSMC simulated carbon dioxide translational temperature (which was found to be equilibrated with the rotational temperature) presented in the left portion of Fig. 12 shows that the near-field agreement corresponding to the onset of condensation is not well described by the simulations for stagnation pressures of 1 and 3 bar.

The inability to model the entire stagnation pressure range of data and the suspicion that the modeling of the release of heat due to condensation might not be correct led to our recent efforts to model condensation directly in BGK.(41) In the first phase, the statistical BGK scheme was implemented in the baseline DSMC code for multi-species and polyatomic gas flows using Eqs. 9 through 18. In the second phase, a new heat addition/accommodation model was incorporated in the BGK and DSMC schemes. The general concept behind the heat addition/accommodation model is that the added heat scales up the random velocities of particles by a factor which is determined by the ratio of heat added per cell per time step and the total random translational energy of all the particles belonging to the cell. The local translational temperature of the cell is then computed based on the scaled up particle velocities. The rotational and vibrational energies also become scaled up because molecular collisions transfer translational to rotational and vibrational energies. The remaining portions of Figs. 11 ((c) and (d)) and 12 (center and right hand side) show the improvement of the new heat addition model. The cluster number density, average cluster size, and the gas temperature close to the condensation onset near the nozzle exit are now in good agreement with the experimental data. The results showing the new heat accommodation model use the BGK simulation, but, the same results (not shown here) for the one and three bar stagnation pressure cases were obtained with the DSMC approach as well. What was not possible to simulate with the DSMC model is the 5 bar case and as Fig. 12 and Ref. (41) show the simulations nicely capture the trends for all measured profiles as a function of stagnation pressure.

Having compared our DSMC and BGK simulations for carbon dioxide condensation with experiment we wanted to see whether we would be able to model a mixture of a carbon dioxide and molecular nitrogen expanding flow. Figure 8(b) shows that the su-
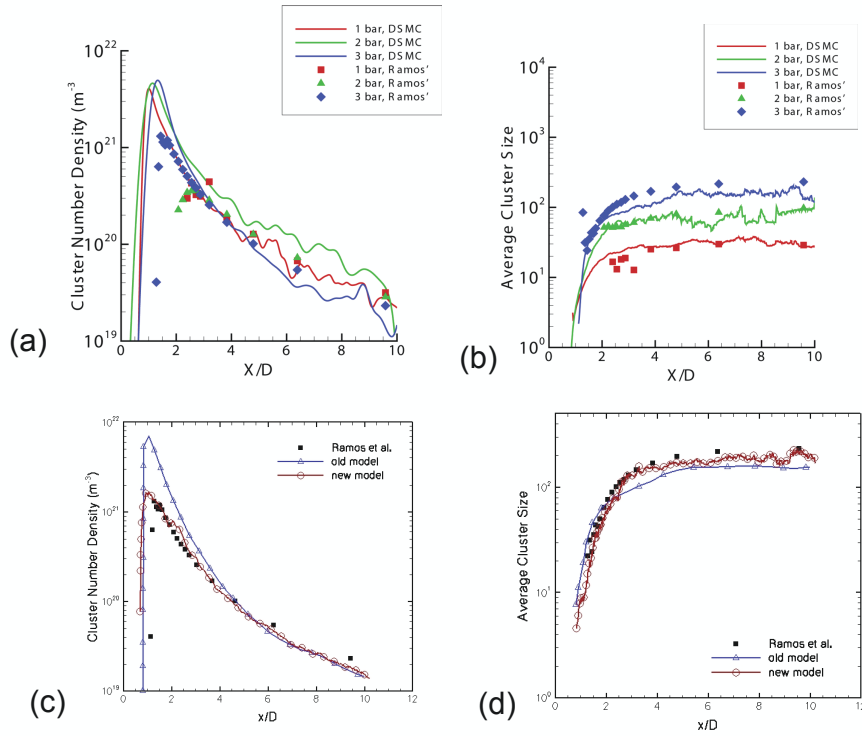
Figure 11: Comparison of cluster number density (a) and (c) and average cluster size (b) and (d) between simulations and experiment. The top row shows the results of DSMC simulations using an older heat addition model. The bottom row shows a comparison of the old versus the new heat addition model and the experiment for the three-bar stagnation case using BGK.
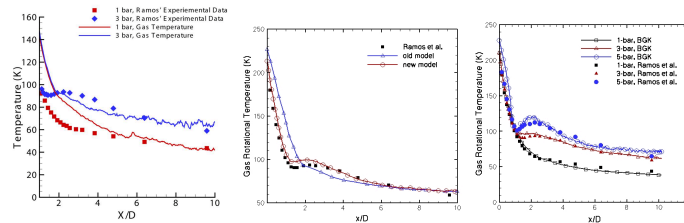

Figure 12: Comparison of gas temperatures. Left figure shows older heat addition results compared to experiment, center figure shows a comparison of older and present results using the new heat addition model for the 3 bar stagnation condition, and right figure shows the comparison of data and new heat addition model for three stagnation pressures.

persaturation ratio reaches unity for carbon dioxide sooner than it does for molecular nitrogen, as expected from common experience. Figure 13(a) shows the potential energy curves for dimers of carbon dioxide and nitrogen. The shallower well for nitrogen compared to carbon dioxide is consistent with its later condensation. The saturation ratio

profiles, S, profiles shown in the figure for the two species corresponds to an expansion from a 15 degree conical nozzle, with throat diameter of 0.6 in, stagnation pressure of 1.02 atm, stagnation temperature of 285 K, and a mixture of 95 N_2 and only 5% CO_2.(28) Because the carbon dioxide condenses prior to nitrogen even a small amount of it will form clusters to then enable nitrogen condensation to occur. This is borne out by the Rayleigh scattering measurements presented in Fig. 13(b) which shows that the pure nitrogen flow is indistinguishable from our DSMC simulated noncondensing flow but when even a trace amount of carbon dioxide gas is added condensation can now be observed.

We proposed that the initial carbon dioxide dimers are created by triple collisions,

$$CO_2 + CO_2 \quad \rightarrow \quad (CO_2)_2^*$$
$$(CO_2)_2^* + N_2 \quad \rightarrow \quad (CO_2)_2 + N_2$$
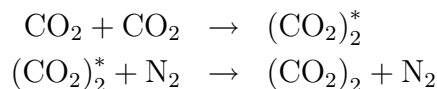
where the triple collision rate depends on the lifetime and collision frequency of the collision complex $(CO_2)_2^*$. The dimer formation probabilities for this process were obtained from MD simulations for temperature conditions that correspond to the nucleation region in the plume. Since the stagnation pressure was sufficiently low, DSMC simulations were performed using generalized cluster-monomer non-sticking collision, condensation, and coalescence models.(40) Figure 13(b) shows that the DSMC simulation that included this condensation mechanism (pink line) compares well with the Rayleigh scattering measurements (green dots).
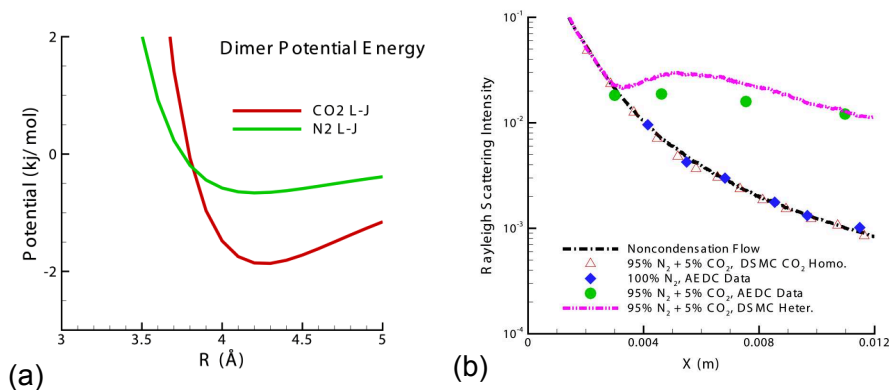

Figure 13: Comparison of Lennard-Jones potential energy curves for carbon dioxide and molecular nitrogen (a) and comparison of Rayleigh scattering measurements with DSMC simulations of heterogeneous carbon dioxide-nitrogen condensating flows (b).

4.3   Ethanol Condensation

Ethanol jet expansions have been studied by Yarygin *et al* as a surrogate for hydrazine back flow contamination.(42) In these experiments they used model thrusters in a vacuum chamber to test the effectiveness of screens in blocking the contaminants from reaching

the backflow area of the plume. Such experiments, while relevant to operational conditions, are difficult to simulate. Instead, we turned to the measurements of Wegener *et al.* (30) who carried out experiments to study homogeneous nucleation of ethanol for varying amounts of ethanol concentration into air at the same total mixture pressure. The conditions for the cases that we modeled are given in Table 1. In our first attempt at simulating these experiments(43) we found that it was not possible to use DSMC to simulate the actual experimental conditions. Therefore an approximation was made in the simulations by assuming that the total mixture pressure was that of the pure ethanol pressure actually used in the experiments, *i.e.*, in Ref. (43) it was assumed that the total pressure was 1.87 kPa instead of the true total pressure of 83.46 kPa. In our more recent work(44) we were able to model the actual experimental conditions using the statistical BGK approach with a condensation models reformulated to take advantage of the BGK approach. The condensation models included CNT-based nucleation and evaporation models as well as coalescence and sticking. In addition a new weighting scheme was implemented to reduce the computational load.

Figure 14 shows the important results of the simulations. Part (a) shows a comparison of our simulated cluster to ethanol gas mass fraction with the experiment for four different ethanol mass fractions as a function of distance from the nozzle exit. Compared to the previous work(43) (seen in (b)) the improvement is quite good. The supersaturation pressure for ethanol as a function of temperature is shown in part (c) to provide a reference for the experimental and simulated condensation onset value. In part (d) we compare our prediction on the condensation onset using the original definition of Wegener *et al* as the location in the flow where the condensed mass fraction reaches 10^{-4}. Both simulated and measured condensation onset occur in the flow at ethanol gas pressures and temperatures above the saturation pressure, as expected. Although the data of Wegener *et al* is old, it is consistent with the more recent data of Wyslouzil *et al*(45). Our numerical results show good agreement with the experiments, thus confirming the use of the BGK based condensation model for computationally challenging high pressure flow applications.

Table 1: Wegener *et al*(30) Experimental Conditions[a]

Case	Ethanol Supply Mass Fraction	Ethanol Partial Pressure (Pa)
1	0.008	211.4
2	0.005	163.5
3	0.0034	89.7
4	0.0025	65.7

[a]Stagnation pressure and temperature are
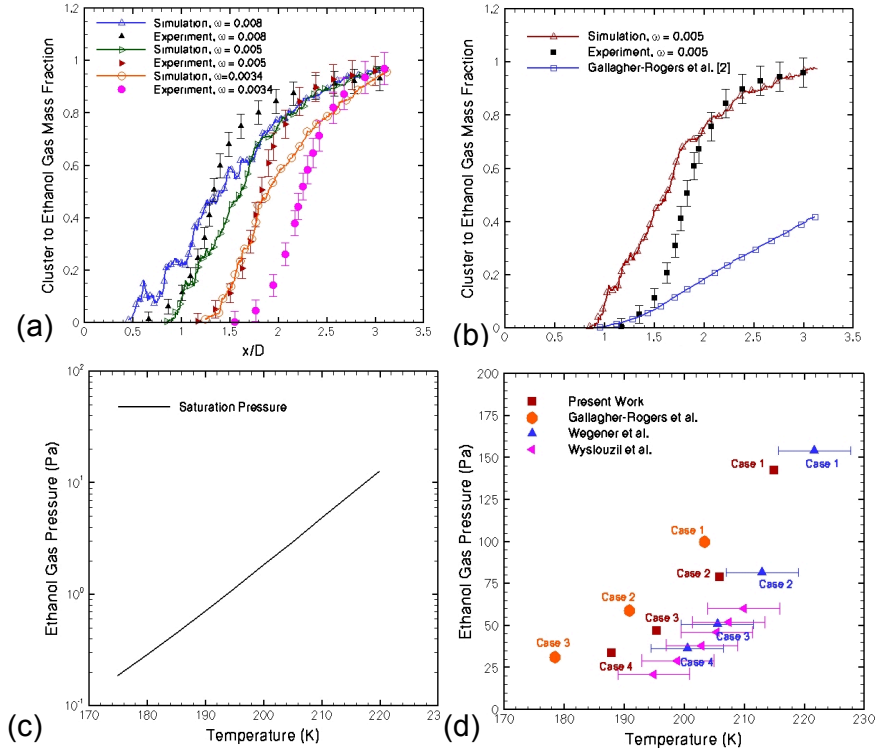83.4 KPa and 296 K, respectively for each case.

Figure 14: Comparison of simulations and measurements of the cluster to ethanol mass fraction for different supply mass fractions of ethanol (a) and our previous modeling (b). The saturation pressure for ethanol is shown in (c) and a comparison of our predicted onset point with data and previous work is presented in (d).

5   Future Directions

The improvements in modeling MEMS and meso-sized propulsion systems in terms of thrust as well as contamination has seen dramatic improvements over the last decade. At the same time, MEMS fabrication techniques have continued to improve leading to higher stagnation pressures while maintaining small sizes. The higher stagnation pressures have the desirable effect of increasing thrust, as expected, and in addition in reducing the large viscous boundary layers at lower stagnation values. While much has been fabricated and demonstrated in a laboratory environment, the non-academic environment has been slow to embrace micro-propulsion even for small satellites. Perhaps the only systems actively being considered today are colloidal micro-thrusters.

Contamination concerns on large satellites are generally handled operationally by sizing and building in extra capacity to meet the mission lifetime requirements. Of course such a strategy will not work for resource limited constellations of small satellites. Moreover, as other forms of propulsion such as electric and mixtures of electric and chemical are considered it can be expected that the spacecraft contamination environment will be even more challenging. New propellants consisting of ionic liquids condensing on spacecraft surfaces in the atomic oxygen low earth orbit environment will present plenty of challenges

to future missions. In terms of modeling and simulation, we are only starting to obtain in inkling of the new chemical models that will be necessary to model contaminating sprays of these advanced propellants.

Acknowledgments

References

[1] Ivanov, M., Kashkovsky, A., Gimelshein, S., Markelov, G., Alexeenko, A., Bondar, Y., Zhukova, G., Nikiforov, S., and Vashenkov, P., "SMILE system for 2D/3D DSMC Computatations," *Proceedings of the 25th International Symposium on Rarefied Gas Dynamics*, 2007.

[2] Jansen, R., Wysong, I., Gimelshein, S., Zeifman, M., and Buck, U., "Nonequilibrium Numerical Model of Homogeneous Condensation in Argon and Water Vapor Expansions," *Journal of Chemical Physics*, Vol. 132, No. 24.

[3] Louisos, W., Alexeenko, A., D.Hitt, and Zilic, A., "Design Considerations for Supersonic Micronozzles," *International Journal of Manufacturing Research*, Vol. 3, No. 1, 2008.

[4] Ketsdever, A., DÕSouza, B., and Lee, R., "Thrust Stand Micromass Balance for the Direct Measurement of Specific Impulse," *J. Propulsion and Power*, Vol. 26, No. 6, 2008.

[5] Ketsdever, A., Young, M., Mossman, J., and Pancotti, A., "Overview of Advanced Concepts for Space Access," *J. Spacecraft and Rockets*, Vol. 47, No. 2, 2010.

[6] Hitt, D., Zakrzwski, C., and Thomas, M., "MEMS-Based Satellite Micropropulsion Via Catalyzed Hydrogen Peroxide Decomposition," *Smart Mater. Struct.*, Vol. 10, 2001.

[7] Bird, G. A., *Molecular Gas Dynamics and the Direct Simulation of Gas Flows*, Clarendon Press, 1994.

[8] Ivanov, M. S. and Rogasinsky, S. V., "Analysis of Numerical Techniques of the Direct Simulation Monte Carlo Method in the Rarefied Gas Dynamics," *Soviet Journal of Numerical Analysis and Mathematical Modeling*, Vol. 3, No. 6, 1988, pp. 453–465.

[9] Alexeenko, A. A., *Modeling of Microscale Gas Flows Using the Direct Simulation Monte Carlo Method*, Ph.D. thesis, The Pennsylvania State University, Pennsylvania, May 2003.

[10] Titov, E. V. and Levin, D. A., "Extension of the DSMC method to High Pressure Flows," *Journal of Computational Fluid Dynamics*, Vol. 21, 2006, pp. 351.

[11] Titov, E., Gallagher-Rogers, A., Levin, D., and Reed, B., "Examination of a Collision-Limiter Direct Simulation Monte Carlo Method for Micropropulsion Applications," *Journal of Propulsion and Power*, Vol. 24, No. 2, March-April 2008.

[12] Kumar, R., Titov, E. V., Levin, D. A., Gimelshein, S. F., and Gimelshein, N. E., "Assessment of Bhatnagar-Gross-Krook Approaches for Near Continuum Regime Nozzle Flows," *AIAA Journal*, Vol. 48, No. 7, 2010.

[13] Gimelshein, S., Alexeenko, A., and Levin, D., "Modeling of the Interaction of a Side Jet with a Rarefied Atmosphere," *Journal of Spacecraft and Rockets*, Vol. 39, No. 2, 2002.

[14] Kumar, R., Titov, E., and Levin, D., "Development of a Particle-Particle Hybrid Scheme Based on ESBGK and DSMC Methods to Simulate Multiscale Transitional Flows," AIAA paper 2011-0625, 2011.

[15] Gallis, M. A. and Torczynski, J. R., "The Application of the BGK Model in Particle Simulations," AIAA paper 2000-2360, 2000.

[16] Holway, L., "Kinetic Theory of Shock Structure using Ellipsoidal Distribution Function," *Proceedings of the Fourth Internation Symposium on Rarefied Gas Dynamics*, 1966, pp. 193–215.

[17] Cercignani, C., "The Boltzmann Equation and its Applications," *Applied Mathematical Sciences*, 1988.

[18] Parker, J., "Rotational and Vibrational Relaxation in Diatomic Gases," *Physics of Fluids*, Vol. 2, 1959, pp. 449–462.

[19] Burt, J. M. and Boyd, I. D., "Evaluation of a Particle Method for the Ellipsoidal Statistical Bhatnagar-Gross-Kroook Equation," *44th AIAA Aerospace Science Meeting and Exhibit, AIAA Paper 2006-989, Reno, Nevada*, January 2006.

[20] Titov, E., R.Kumar, and Levin, D., "Assessment of Kinetic BGK Application to the Internal and External Flows in Modeling RCC Crack Growth," AIAA paper 2009-3756, 2009.

[21] Allen, M. and Tildesley, D., *Computer simulation of Liquids*, Oxford University Press, 1987.

[22] Reed, B., de Groot, W., and Dang, L., "Experimental Evaluation of Cold Flow Micronozzles," *AIAA Paper No. 2001-3521*, July 2001.

[23] Alexeenko, A., Levin, D., Gimelshein, S., Collins, R., and Markelov, G., "Numerical Simulation of High-Temperature Gas Flows in a Millimeter-Scale Thruster," *Journal of Thermophysics and Heat Transfer*, , No. 1, January-March 2002.

[24] Alexeenko, A., Levin, D., Fedosov, D., Gimelshein, S., and Collins, R., "Performance Analysis of Microthrusters Based on Coupled Thermal-Fluid Modeling and Simulation," *Journal of Propulsion and Power*, Vol. 21, No. 1, 2005.

[25] Alexeenko, A., Fedosov, D., Gimelshein, S., Levin, D., and Collins, R., "Transient Heat Transfer and Gas Flow in a MEMS-Based Thruster," *Journal of Microelectromechanical Systems*, Vol. 15, 2006.

[26] Kandlikar, S. and Steike, M., "Predicting Heat Transfer During Flow Boiling in Minichannels and Microchannels," *ASHRAE Transactions*, Vol. 109, No. 1, 2003.

[27] Hagena, O. F. and Obert, W., "Cluster Formation in Expanding Supersonic Jets: Effect of Pressure, Temperature, Nozzle Size, and Test Gas," *J. Chem. Phys.*, Vol. 56, 1972, pp. 1793.

[28] Williams, W. and Lewis, J., "Summary report for the CONSET program at AEDC," *Arnold Engineering Development Center*, , No. AEDC-TR-80-16, 1980.

[29] Ramos, A., Fernández, J. M., Tejeda, G., and Montero, S., "Quantitative Study of Cluster Growth in Free-jet Expansions of CO_2 by Rayleigh and Raman scattering," *Physical Review A*, Vol. 72, No. 5, 2005, pp. 3204–3210.

[30] Wegener, P. P., Clumpner, J. A., and Wu, B. J. C., "Homogeneous Nucleation and Growth of Ethanol Drops in Supersonic Flow," *The Physics of Fluids*, Vol. 15, No. 11, November 1972, pp. 1869–1876.

[31] Li, Z., Zhong, J., Levin, D., and Garrison, B., "Development of Homogeneous Water Condensation Models Using Molecular Dynamics," *AIAA Journal*, Vol. 47, No. 5, May 2009.

[32] Li, Z., Zhong, J., Levin, D., and Garrison, B., "Kinetic Nucleation Model for Free-Expanding Water Condensation Plume Simulations," *Journal of Chemical Physics*, Vol. 130, No. 17, May 2009.

[33] Li, Z. and Levin, D., "Development of a Molecular Dynamics-based Coalescence Model for DSMC Simulations of Ammonia Condensate Flows," *Submitted for publication to the Journal of Chemical Physics, Nov. 2010*.

[34] Bobbert, C., Schutte, S., Steinbach, C., and Buck, U., "Fragmentation and Reliable Size Distributions of Large Ammonia and Water Clusters," *European Physical Journal D*, Vol. 19, No. 2, 2002, pp. 183–192.

[35] Zhong, J., Zeifman, M., and Levin, D., "Sensitivity of Water Condensation in a Supersonic Plume to the Nucleation Rate," *Journal of Thermophysics and Heat Transfer*, July-September 2006, pp. 517–523.

[36] Abraham, F., *Homogeneous Nucleation Theory: The Pretransition Theory of Vapor Condensation*, Academic Press, New York, 1974.

[37] Zhong, J., *The Modeling of Homogeneous Condensation in Free-Expanding Plumes with the Direct Simulation Monte Carlo Method*, Ph.D. thesis, The Pennsylvania State University, Pennsylvania, May 2005.

[38] Zhong, J. and Levin, D., "Development of a Kinetic Nucleation Model for a Free-Expanding Argon Condensation Flow," *AIAA Journal*, Vol. 45, No. 4, 2007.

[39] Zhong, J., Zeifman, M. I., and Levin, D. A., "Kinetic Model of Condensation in a Free Argon Expanding Jet," *Journal of Thermophysics and Heat Transfer*, Vol. 20, No. 1, 2006, pp. 41–51.

[40] Li, Z., Zhong, J., and Levin, D. A., "Modeling of CO_2 Homogeneous and heterogeneous Condensation Plumes," *The Journal of Physical Chemistry, special edition*, 2009.

[41] Kumar, R. and Levin, D., "Simulation of Homogeneous Condensation of Small Polyatomic Systems in High Pressure Supersonic Nozzle Flows using the BGK Model," *Submitted to The Journal of Chemical Physics*, 2010.

[42] Yarygin, V., Prikhodko, V., Yarygin, I., Gerasimov, Y., and Krylov, A., "Gas-Dynamic Aspects of the Contamination Problem at the International Space Station 1.Model Experiments," *Thermophysics and Aerodynamics*, Vol. 10, No. 2, 2003, pp. 269–286.

[43] Gallagher-Rogers, A., Zhong, J., and Levin, D., "Simulation of Homogeneous Ethanol Condensation in Supersonic Nozzle Flows using DSMC," *39th AIAA Thermophysics Conference, AIAA Paper No. 2007-4159, Miami, Florida, submitted to the Journal of Thermophysics and Heat Transfer*, 25-28 June 2007.

[44] Kumar, R. and Levin, D., "Simulation of Homogeneous Condensation of Ethanol in High Pressure Supersonic Nozzle Flows using BGK Condensation Model," *Submitted to AIAA Journal*, 2010.

[45] Wyslouzil, B., Heath, C., and Cheung, J., "Binary Condensation in a Supersonic Nozzle," *Journal of Chemical Physics*, Vol. 113, No. 17, November 2000, pp. 7317–7329.

[46] Ivanov, M. and Gimelshein, S., "Current Status and Prospects of the DSMC Modeling of Near-Continuum Flows of Non-reacting and Reacting Gases," *Proceedings of the Rarefied Gas Dynamics 23rd Int. Symp., AIP Conference*, Vol. 663, 2003, pp. 339–348.